https://doi.org/10.1016/j.combustflame.2021.111859

Thermoacoustic modal instability and its suppression with locally resonant flexible membranes

Yang Liu[a], Jingtao Du[a,b], Li Cheng*[, b]

[a]*College of Power and Energy Engineering, Harbin Engineering University, Harbin, 150001, China*

[b]*Department of Mechanical Engineering, The Hong Kong Polytechnic University, Hong Kong, 999077, China*

*Corresponding author.

E-mail address: li.cheng@polyu.edu.hk (L. Cheng)

ABSTRACT

Thermoacoustic oscillation and instability are a common occurrence in many industrial problems. Investigations on the interplay among different types of modes, their evolution process and coupling with add-on control devices are of vital importance to guide the development of proper control strategies. Using a linear heat release n-τ model inside a duct, these issues are investigated in this paper based on a fully coupled energy-based model. Studies allow the classification and quantification of different types of eigen-modes, as well as their stability and controllability features. Using flush-mounted flexible membranes over the duct wall, possible suppressions of instable modes and the underlying control mechanisms are revealed. Numerical analyses show that thermoacoustic instability of the system can be controlled via creating strong vibro-acoustic coupling, but via two different physical mechanisms for acoustic and intrinsic modes. For the former, the acoustic modal pressure distribution should be positively altered in the vicinity of the heat source to create a favorable pressure state scenario. For the latter, control is achieved indirectly through a proper alteration of the nearby acoustic modes, thus affecting their coupling with the targeted intrinsic mode. In both cases, a successful suppression of the thermoacoustic modal instability can be materialized through a proper adjustment of the physical parameters of the membranes and their installation locations.

Keywords: Thermoacoustic oscillation; n-τ model; intrinsic mode; modal instability control

1. Introduction

Thermoacoustic oscillation occurs in many engineering systems such as industrial furnaces, gas turbines and rocket engines etc. For example, the premixed combustion in a low emission combustor system can cause thermoacoustic instability [1-3]. As experimentally illustrated in a Rijke tube, a heating wire mesh placed at the lower part of a vertical empty pipe with both ends open may arouse strong self-excited oscillations inside the tube [4]. This happens because the unsteady heating generates sound waves, and part of upstream-travelling waves in turn perturb the input rate of the heat source. As a result, instability is triggered when the phase relationship is such that the unsteady rate of the heat input and the pressure perturbations is positively enhanced [5]. For a simplified flame model, such as the n-τ flame model [6], the heat release rate is usually proportional to the medium volume expansion rate as the viscosity and heat conduction are ignored.

The physical mechanism underpinning the thermoacoustic oscillation has been revealed in the literatures with the consideration of temperature gradient, mean flow effect or complex combustion states [7-9]. It was demonstrated that the standing-waves of acoustic modes may become unstable, which depends on the phase relationship of the acoustic pressure and the flame [10]. More specifically, instability may be triggered when the heat source is placed at those locations where the sound pressure is strengthened [11], which also implies that the acoustic modal characteristics have significant influence on the thermoacoustic oscillation.

Due to the frequent occurrence of thermoacoustic oscillation and its practical implication in a combustion system, developing effective strategies for instability control has always been an important research topic. Existing means include both active or passive techniques. As a typical example, Heckl [12] studied the active control of the thermoacoustic oscillation in a Rijke tube. The concept of using feedback control to alter the interaction between the acoustic waves and the unsteady heat release was introduced by Dowling and Morgans [13]. Towards increasing efficiency and the capability, a specific feedback control using a time-delayed integral algorithm was proposed by Olgac and Zalluhoglu [14]. Despite the appealing adaptive feature it offers,

active control usually involves complex electronics, high cost alongside stability concern. Therefore, passive control still remains as an important alternative for the thermoacoustic instability control.

Helmholtz resonator (HR) is a simple and effective device to suppress the thermoacoustic oscillation [15]. Past efforts include the design of its cavity size, aperture length/width and the use of multiple HRs in various combustion systems [16-18] including in complex sound environment such as flow medium [19]. In addition to HRs, perforated liners have also attracted immense attention [20-22]. Compared with HRs, a perforated liner in a flow duct allows for a compact structural design and a significant damping enhancement at the same time. Besides, attempts were made through embedding elastic membranes on a duct sidewall, whose configuration was determined through sophisticated numerical analyses and optimizations [23]. Irrespective of the methods used, passive or active, the essence of a successful control is to create positive changes in the acoustic field so as to further alter the interaction of acoustic waves and unsteady heat release. A prerequisite to achieve this goal is a good understanding on the physical properties of the system instability and their interplay with other system parameters characterized by various acoustic/thermal metrics.

One of the important issues in thermoacoustic research is the classification and the apprehension of the interplay of different types of oscillation modes existing in a thermoacoustic system. The topic has been arousing an increasing research interest in recent years. In addition to the conventional acoustic modes, a new type of modes which are tidily associated with the heat source are shown to be of particular importance. Hoeijmakers and Emmert *et al.* [24-26] reported that a flame (based on a linear n-τ heat release model) can be an intrinsically unstable element, which is shown to become dominant in the extreme case with no acoustic reflections at the boundaries. It was suggested that the flame, as a subsystem in a combustor, can give rise to a completely new family of modes, referred to as flame intrinsic modes. The flame, in return, reacts on the acoustic velocity created by itself and thus forms a local feedback loop, possibly unstable. The stabilities of the intrinsic and acoustic modes are closely related to the flame interaction index n and the time-lag τ. For a small n, these intrinsic modes are strongly damped, while they become unstable only if n exceeds a certain threshold

[27-28]. Mukherjee studied the coupling between the acoustic and intrinsic modes. Results show that for a small n, the eigenfunctions of adjacent acoustic and flame intrinsic modes clearly exhibit distinctive properties [29]. More complex combustion flame model such as turbulent spray flame was also studied by Emmert and Ghani *et al.* [30-31] to discern acoustic and intrinsic eigenmodes in a combustor test rig, in particular the corresponding mode shapes. Buschmann and Orchini *et al.* [32-33] proposed a distinction between "intrinsic thermoacoustic driven" and "acoustic driven" thermoacoustic modes. The concept of exceptional points (EPs) was also proposed to give a qualitative prediction and understanding of the eigenvalue trajectories of thermoacoustic systems for different parameters. It was shown that the intrinsic modes, distinctly different from the acoustic modes, are important to be considered. However, existing literature mainly focuses on the intrinsic/acoustic modal characteristics and their instability features. An in-depth understanding of the interplay among these modes, their evolution process and the coupling mechanism with add-on control devices need more thorough investigations. This is vital to guide the development and the implementation of proper control strategies, as well as to understand the underlying thermoacoustic instability suppression mechanisms.

The above analyses motivate the present work. In particularly, characteristics of intrinsic and acoustic modes in a duct, as well as the thermoacoustic instability control mechanism using locally resonant flexible membranes, are systematically investigated. The analyses are based on a proposed energy-based semi-analytical model involving a conventional linear n-τ flame model. Then, a locally resonant flexible membrane is flush-mounted inside the duct wall as a control device. Numerical studies demonstrate the controllability of intrinsic and acoustic modes and reveal the underlying control mechanism. Different from HRs or other devices, the membrane contains multiple modes within a certain frequency band [34-35], which offers the possibility of simultaneously controlling multiple instable modes.

The remaining part of the paper is organized as follows. A theoretical formulation on the problem under investigation is first presented in Section 2. In the results and discussion section 3, the first part presents a thorough analysis on the behaviors of intrinsic and acoustic modes, followed by the second part on the coupling characteristics between the control device and

acoustic modes in a duct. Numerical analyses show the control effect, its underlying mechanism and the corresponding changes on different unstable acoustic modes and intrinsic modes, respectively. Finally, conclusions are drawn.

2. THEORETICAL FORMULATION

2.1. Modelling of a flame coupled with the acoustic field inside a duct

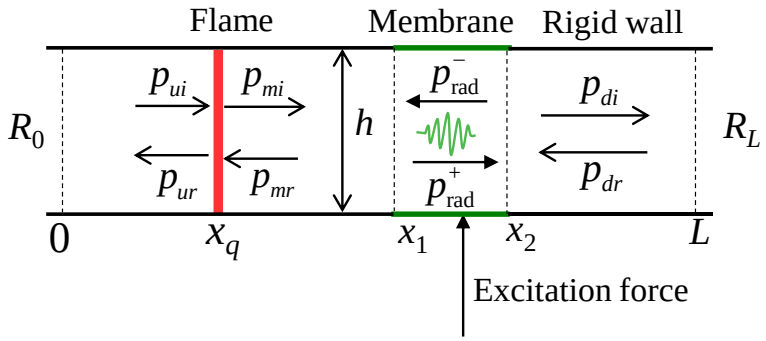

Fig. 1. Schematic diagram of a flame-duct-membrane thermoacoustic coupling model

Consider the thermoacoustic oscillation inside a duct system illustrated in Fig. 1. The system consists of a flame and the sound field inside the duct, a segment of which is symmetrically formed by thin membranes (from x_1 to x_2) as a device to control the system instability. The duct (length L, height h) has two ends with reflection coefficients denoted as R_0 and R_L, respectively. A compact flame is located at $x=x_q$, with a heat release rate $q'(x, t)=Q'(t)\delta(x-x_q)$, where $Q'(t)=Qe^{-i\omega t}$ and δ denotes the Dirac δ-function. The entire system is segmented into five portions, namely three duct segments with rigid walls, a flame area, and the embedded membrane, as depicted in Fig.1.

The acoustic filed in the vicinity of the heat source is first modelled by adopting the plane wave theory, applicable to frequencies below the cut-on frequency of the duct. In the flame region, the sound pressure and velocity waves across the flame can be expressed as

$$p_{ui} = A'e^{-ik^- x},\quad p_{ur} = B'e^{ik^- x},\quad p_{mi} = C'e^{-ik^+ x},\quad p_{mr} = D'e^{ik^+ x} \tag{1}$$

$$v_{\mathrm{ui}}=\frac{A'}{\rho^{-}c^{-}}\mathrm{e}^{-\mathrm{i}k^{-}x},\ v_{\mathrm{ur}}=-\frac{B'}{\rho^{-}c^{-}}\mathrm{e}^{\mathrm{i}k^{-}x},\ v_{\mathrm{mi}}=\frac{C'}{\rho^{+}c^{+}}\mathrm{e}^{-\mathrm{i}k^{+}x},\ v_{\mathrm{mr}}=-\frac{D'}{\rho^{+}c^{+}}\mathrm{e}^{\mathrm{i}k^{+}x} \tag{2}$$

where, the subindices r denotes "reflected" and i means "incident". $k=\omega/c$ is the acoustic wave number; ω angular frequency; c sound speed; ρ air density. The symbols "−"and "+" represent the parameters before and after the heat source, respectively. Assuming an uniform temperature at the flame, then one has $k^{-}=k^{+}=k$, $c^{-}=c^{+}=c$ and $\rho^{-}=\rho^{+}=\rho$. A', B', C' and D' are the unknown coefficients to be determined. Using the momentum and mass conservation principle, one has

$$\left[p\right]_{x=x_q^-}^{x=x_q^+}=0 \tag{3}$$

$$\left[\rho v\right]_{x=x_q^-}^{x=x_q^+}=\frac{(\gamma-1)}{(c^{-})^2}Q(\omega)\mathrm{e}^{-\mathrm{i}\omega t} \tag{4}$$

A linear $n-\tau$ flame model is adopted [6], with the coefficient of heat release rate written as

$$Q(\omega)=\frac{\rho^{-}c^{-}}{\gamma-1}n\mathrm{e}^{\mathrm{i}\omega\tau}(v_{\mathrm{ui}}+v_{\mathrm{ur}})\Big|_{x_{\mathrm{q}}} \tag{5}$$

in which, n and τ correspond to the flame interaction index and time-lag, respectively; γ denotes the specific heat ratio and the product $n\mathrm{e}^{\mathrm{i}\omega\tau}$ is the flame transfer function (FTF), $F(\omega)$.

Combining Eqs. (1-5) and ignoring the temperature jump across the heat source yield the following two linear equations in terms of the unknown coefficients A', B', C' and D':

$$A'\mathrm{e}^{-\mathrm{i}k^{-}x_{\mathrm{q}}}+B'\mathrm{e}^{\mathrm{i}k^{-}x_{\mathrm{q}}}=C'\mathrm{e}^{-\mathrm{i}k^{+}x_{\mathrm{q}}}+D'\mathrm{e}^{\mathrm{i}k^{+}x_{\mathrm{q}}} \tag{6}$$

$$C'\mathrm{e}^{-\mathrm{i}k^{+}x_{\mathrm{q}}}-D'\mathrm{e}^{\mathrm{i}k^{+}x_{\mathrm{q}}}-(A'\mathrm{e}^{-\mathrm{i}k^{-}x_{\mathrm{q}}}-B'\mathrm{e}^{\mathrm{i}k^{-}x_{\mathrm{q}}})=F(\omega)(A'\mathrm{e}^{-\mathrm{i}k^{-}x_{\mathrm{q}}}-B'\mathrm{e}^{\mathrm{i}k^{-}x_{\mathrm{q}}}) \tag{7}$$

The right-hand-side part of Eq. (7) is the velocity fluctuation generated by the unsteady rate of the flame heat release. When the up-travelling part is in phase with the pressure perturbation, acoustic wave gains energy and the system will become instable [6]. The sound pressure in the downstream near the right end can be written as

$$p_{\mathrm{di}}=E'\mathrm{e}^{-\mathrm{i}kx},\qquad p_{\mathrm{dr}}=F'\mathrm{e}^{\mathrm{i}kx} \tag{8a, b}$$

In light of the boundary conditions, the relationship among p_{ui}, p_{ur} and p_{di}, p_{dr} can be written as

$$\frac{p_{\mathrm{ui}}(0)}{p_{\mathrm{ur}}(0)}=R_0=\frac{A'}{B'} \tag{9}$$

$$\frac{p_{\mathrm{di}}(L)}{p_{\mathrm{dr}}(L)} = R_L = \frac{E'\mathrm{e}^{-\mathrm{i}kL}}{F'\mathrm{e}^{\mathrm{i}kL}} \tag{10}$$

In the absence of the membrane, one will have $p_{\mathrm{di}}=p_{\mathrm{mi}}$, $p_{\mathrm{dr}}=p_{\mathrm{mr}}$. Combining Eqs. (6), (7), (9) and (10) yields four homogeneous equations in terms of the four amplitude unknowns A', B', C' and D'. To get nontrivial solutions of the eigen-problem cast into the aforementioned four equations, the determinant of the coefficient matrix needs to be zero. Then, the eigenroots ω for the thermoacoustic coupling system can be obtained.

2.2. Sound propagation around the locally resonant membrane

While plane wave propagation can be considered in the rigid segments of the duct below its cut-on frequency, higher order duct modes need to be considered for the flexible membrane part, thus resulting in a coupling between the duct and the membrane. In this section, an energy-based approach is followed to capture this vibro-acoustic coupling behavior. The transverse displacement of the flexible membrane with fixed boundaries can be expanded as

$$w(x) = \sum\nolimits_{q=1}^{S} a_q \sin(q\pi x/L_m) = \mathbf{\Psi}(x)\mathbf{A} \tag{11}$$

in which, S is the truncation number of Fourier series and L_m the membrane length; $\mathbf{\Psi}$ denotes the mode shape vector. The Lagrangian of the membrane writes

$$L_{\mathrm{memb}} = U_{\mathrm{memb}} - T_{\mathrm{memb}} + W_{\mathrm{P}} + W_{\mathrm{F}} \tag{12}$$

where the subscript "memb" is the abbreviation of membrane. U_{memb} and T_{memb} denote the total potential and kinetic energies, respectively; W_{P} represents the work done by the sound pressure inside the duct over the upper surface of the membrane; W_{F} represents the work done by the excitation force, namely [35]

$$U_{\mathrm{memb}} = \frac{1}{2}T\int_0^{L_{\mathrm{m}}}\left[\frac{\partial w(x)}{\partial x}\right]^2 \mathrm{d}x, \qquad T_{\mathrm{memb}} = \frac{1}{2}\omega^2\rho_{\mathrm{m}}\int_0^{L_{\mathrm{m}}} w^2(x)\mathrm{d}x \tag{13a, b}$$

$$W_{\mathrm{p}} = \int_0^{L_{\mathrm{m}}}\left(p_{\mathrm{rad}}+p_{\mathrm{mi}}+p_{\mathrm{dr}}\right)w\mathrm{d}x, \qquad W_{\mathrm{F}} = \int_0^{L_{\mathrm{m}}} f_{\mathrm{exc}}w\delta(x\text{-}x_{\mathrm{s}})\mathrm{d}x \tag{14a, b}$$

in which T and ρ_{m} correspond to the tension applied to the membrane and its mass density, respectively. f_{exc} is an excitation force exerted on the membrane at the position x_{s}. p_{rad} is the sound pressure radiated by the membrane in the duct, which can be estimated [36]

$$p_{\mathrm{rad}}(x,y)=\frac{\rho}{2h}\sum_{m=0}^{\infty}\frac{\omega}{k_m}\psi_m(y)\int_0^{L_{\mathrm{m}}}\psi_m(y_{\mathrm{s}})\Big|_{y_{\mathrm{s}}=0}\mathrm{i}\omega w\times G(x,x')\mathrm{d}x' \tag{15}$$

where $\psi_m(y)$ is the acoustic mode shape function of the duct, G (x, x') and k_m are Green's function and modal wavenumber, respectively, defined as

$$\psi_m(y)=\sqrt{2-\delta_{0m}}\cos\left(\frac{m\pi}{h}y\right),\quad \begin{matrix}G=H(x-x')\mathrm{e}^{-\mathrm{i}k_m(x-x')}\\ +H(x'-x)\mathrm{e}^{+\mathrm{i}k_m(x-x')}\end{matrix},\ k_m=\frac{\omega}{\mathrm{i}c}\sqrt{\left(m\pi/k_0h\right)^2-1} \tag{16a, b, c}$$

where H is the Heaviside function. Zero-order plane wave corresponds to m=0, while higher-order modes correspond to m>1. Combining Eqs. (11)-(15) and using Lagrange's equations $\frac{\mathrm{d}}{\mathrm{d}t}\left(\frac{\partial L}{\partial \dot{a}_q(t)}\right)-\frac{\partial L}{\partial a_q(t)}=0$ and under harmonic regime for the modal amplitude coefficients a_q yield a set of linear equations, which can be written in a matrix form as

$$(\mathbf{K}-\omega^2\mathbf{M}+\mathrm{i}\omega\mathbf{G})\mathbf{a}=\mathbf{P}_{\mathrm{i\&r}}+\mathbf{F} \tag{17}$$

The unknown modal amplitude response vector can then be determined as [38, 39]

$$\mathbf{a}=\left(\mathbf{K}-\omega^2\mathbf{M}+\mathrm{i}\omega\mathbf{G}\right)^{-1}\left(\mathbf{P}_{\mathrm{i\&r}}+\mathbf{F}\right)=\mathbf{\Pi}\left(\mathbf{P}_{\mathrm{i\&r}}+\mathbf{F}\right) \tag{18}$$

in which $\mathbf{K}$ and $\mathbf{M}$ are the stiffness and mass matrices of the flexible membrane *in vacuo*, respectively; $\mathbf{G}$ is the coupling matrix characterizing the membrane-duct interaction; $\mathbf{F}$ is the load vector originating from the excitation force. Vector $\mathbf{P}_{\mathrm{i\&r}}$ denotes the work done by plane wave p_{mi} and p_{dr}. The solution of Eq. (18) gives the modal amplitude vector $\mathbf{a}$, thus allowing the calculation of all the other vibro-acoustic metrics.

2.3. Interaction between the thermoacoustic system and the resonant membranes

For the sound field inside the duct in the presence of a flame, the load vector $\mathbf{P}_{\mathrm{i\&r}}$ in Eq.(18) is related to the boundary conditions and the flame heat release, which can be further expressed as

$$\mathbf{P}_{\mathrm{i\&r}}=p_{\mathrm{mi}}(x_1)\mathbf{P}_1+p_{\mathrm{dr}}(x_2)\mathbf{P}_2 \tag{19}$$

in which,

$$\left\{\mathbf{P}_1\right\}_q=\mathrm{e}^{-\mathrm{i}kx_1}\int_0^{L_{\mathrm{m}}}\left\{\mathbf{\Psi}\right\}_q\mathrm{e}^{-\mathrm{i}kx}\mathrm{d}x,\qquad \left\{\mathbf{P}_2\right\}_q=\mathrm{e}^{\mathrm{i}kx_2}\int_0^{L_{\mathrm{m}}}\left\{\mathbf{\Psi}\right\}_q\mathrm{e}^{-\mathrm{i}kx}\mathrm{d}x \tag{20a, b}$$

where, the brackets $\{\}_q$ indicates the q-order term in the vectors $\mathbf{P}$ and $\mathbf{\Psi}$. The continuity condition of the sound pressure at the cross-sections x_1 and x_2 gives

$$p_{\mathrm{mr}}(x_1) = p_{\mathrm{dr}}(x_2)\mathrm{e}^{-\mathrm{i}kL_m} + p_{\mathrm{rad}}^{-}(x_1), \qquad p_{\mathrm{di}}(x_2)=p_{\mathrm{mi}}(x_1)\mathrm{e}^{-\mathrm{i}kL_m}+p_{\mathrm{rad}}^{+}(x_2) \tag{21a, b}$$

in which, p_{rad}^{+} and p_{rad}^{-} are the pressure waves radiated by membrane in *x*-positive and negative directions. When the excitation frequency is much lower than the cut-on frequency of the duct, the radiated sound wave that propagates into the far-field, both upstream or downstream along the duct, is largely dominated by the zero-order wave, namely the plane sound wave. Then, the radiation waves p_{rad}^{+} and p_{rad}^{-} can be written in the following simplified form based on Eq.15,

$$p_{\mathrm{rad}}^{+} = \mathrm{e}^{-\mathrm{i}kL_m}\frac{\rho c}{2h}\int_0^{L_m}\mathrm{i}\omega w(x')\mathrm{e}^{\mathrm{i}kx'}\mathrm{d}x' = \mathbf{P}^{+}\boldsymbol{\Pi}(\mathbf{P}_{\mathrm{i\&r}}+\mathbf{F}) \tag{22}$$

$$p_{\mathrm{rad}}^{-} = \frac{\rho c}{2h}\int_0^{L_{\mathrm{m}}}\mathrm{i}\omega w(x')\mathrm{e}^{-\mathrm{i}kx'}\mathrm{d}x' = \mathbf{P}^{-}\boldsymbol{\Pi}(\mathbf{P}_{\mathrm{i\&r}}+\mathbf{F}) \tag{23}$$

where,

$$\left\{\mathbf{P}^{+}\right\}_q = \mathrm{e}^{-\mathrm{i}kL}\mathrm{i}\omega\frac{\rho c}{2h}\int_0^{L_{\mathrm{m}}}\left\{\boldsymbol{\psi}\right\}_q\mathrm{e}^{\mathrm{i}kx}\mathrm{d}x \tag{24}$$

$$\left\{\mathbf{P}^{-}\right\}_q = \mathrm{i}\omega\frac{\rho c}{2h}\int_0^{L_{\mathrm{m}}}\left\{\boldsymbol{\psi}\right\}_q\mathrm{e}^{-\mathrm{i}kx}\mathrm{d}x \tag{25}$$

Combining Eqs. (19), (21), (22) and (23) yields

$$\mathbf{P}^{-}\boldsymbol{\Pi}\mathbf{P}_1 p_{\mathrm{mi}}(x_1) - p_{\mathrm{mr}}(x_1) = -(\mathrm{e}^{-\mathrm{i}kL_m}+\mathbf{P}^{-}\boldsymbol{\Pi}\mathbf{P}_2)p_{\mathrm{dr}}(x_2) - \mathbf{P}^{-}\boldsymbol{\Pi}\mathbf{F} \tag{26}$$

$$(\mathrm{e}^{-\mathrm{i}kL_m}+\mathbf{P}^{+}\boldsymbol{\Pi}\mathbf{P}_1)p_{\mathrm{mi}}(x_1) = p_{\mathrm{di}}(x_2) - \mathbf{P}^{+}\boldsymbol{\Pi}\mathbf{P}_2 p_{\mathrm{dr}}(x_2) - \mathbf{P}^{+}\boldsymbol{\Pi}\mathbf{F} \tag{27}$$

Using Eqs. (26) and (27) and combining the flame Eqs. (6) and (7) alongside the boundary conditions Eqs. (9) and (10), one can obtain six equations in terms of six unknown coefficients A', B', C', D', E' and F', cast into a matrix form, namely

$$\begin{bmatrix} -1 & R_0 & 0 & 0 & 0 & 0 \\ \mathrm{e}^{-\mathrm{i}kx_{\mathrm{q}}} & \mathrm{e}^{\mathrm{i}kx_{\mathrm{q}}} & -\mathrm{e}^{-\mathrm{i}kx_{\mathrm{q}}} & -\mathrm{e}^{\mathrm{i}kx_{\mathrm{q}}} & 0 & 0 \\ (1+n\mathrm{e}^{\mathrm{i}\omega\tau})\mathrm{e}^{-\mathrm{i}kx_{\mathrm{q}}} & (-1-n\mathrm{e}^{\mathrm{i}\omega\tau})\mathrm{e}^{\mathrm{i}kx_{\mathrm{q}}} & -\mathrm{e}^{-\mathrm{i}kx_{\mathrm{q}}} & \mathrm{e}^{\mathrm{i}kx_{\mathrm{q}}} & 0 & 0 \\ 0 & 0 & \Gamma_{11} & \Gamma_{12} & \Gamma_{13} & \Gamma_{14} \\ 0 & 0 & \Gamma_{21} & \Gamma_{22} & \Gamma_{23} & \Gamma_{24} \\ 0 & 0 & 0 & 0 & -\mathrm{e}^{-\mathrm{i}kL} & R_{\mathrm{L}}\mathrm{e}^{\mathrm{i}kL} \end{bmatrix}\begin{bmatrix} A' \\ B' \\ C' \\ D' \\ E' \\ F' \end{bmatrix} = \boldsymbol{\Lambda}\begin{bmatrix} A' \\ B' \\ C' \\ D' \\ E' \\ F' \end{bmatrix} = \begin{bmatrix} 0 \\ 0 \\ 0 \\ -\mathbf{P}^{+}\boldsymbol{\Pi}\mathbf{F} \\ -\mathbf{P}^{-}\boldsymbol{\Pi}\mathbf{F} \\ 0 \end{bmatrix} \tag{28}$$

The elements marked as Γ are determined by Eqs. (26) and (27), which can be expressed as

$$\Gamma_{11}=\mathbf{P}^{-}\boldsymbol{\Pi}\mathbf{P}_1\mathrm{e}^{-\mathrm{i}kx_1},\ \Gamma_{12}=-\mathrm{e}^{\mathrm{i}kx_1},\ \Gamma_{13}=0,\ \Gamma_{14}=(\mathrm{e}^{-\mathrm{i}kL_m}+\mathbf{P}^{-}\boldsymbol{\Pi}\mathbf{P}_2)\mathrm{e}^{\mathrm{i}kx_2} \tag{29}$$

$$\Gamma_{21}=(e^{-ikL_m}+\mathbf{P}^{+}\mathbf{\Pi}\mathbf{P}_1)e^{-ikx_1},\ \Gamma_{22}=0,\ \Gamma_{23}=-e^{-ikx_2},\ \Gamma_{11}=\mathbf{P}^{+}\mathbf{\Pi}\mathbf{P}_2e^{ikx_2} \quad (30)$$

The right-hand-side part of the Eq. 28 is the excitation term, which is independent of the thermoacoustic system.

Eq.28 is applicable when a membrane is deployed behind the flame. Otherwise, the coefficient matrix should be re-arranged. In the above equation, ω is an unknown variable. All the roots can be solved via setting the determinant of the coefficient matrix $\mathbf{\Lambda}$ to be zero. Due to the existence of the heat source, these frequencies are generally complex, namely $\omega=\omega_r+i\omega_i$, in which the real part ω_r is the natural frequency of the thermoacoustic coupling system, and the imaginary ω_i is the growth rate (GR) of the mode characterizing its stability nature. When ω_i is negative, the heat disturbance disappears in a short time. However, if ω_i is positive, the system oscillation will grow exponentially with time and eventually lead to system instability. A numerical procedure is used to obtain the eigen-solutions of the above system, and the behaviour of the acoustic and intrinsic modes is illustrated by contour plots in the complex frequency plane. For any given variation range of ω, *e.g.* $Re\{\omega\}$ from 0~6000 rad/s and $Im\{\omega\}$ from −600~300 rad/s, with a step size $\triangle$=1 rad/s, the modal frequencies are determined when $|\mathbf{\Lambda}(\omega)|=0$.

3. Results and discussions

3.1 Modal characteristics analysis of thermoacoustic system

Thermoacoustic instability originates from the coupling between the flame heat release and certain acoustic modes of the duct, which has been well defined in the literature. Recent study shows that this may also happen even if the boundary reflection coefficient of the duct is set to be infinitesimal [24]. Such instability is due to the local feedback loop formed by the flame heat source itself. The natural modes of the system formed by the local feedback loop of the flame are referred to as intrinsic modes hereafter.

In this section, the intrinsic/acoustic modal characteristics of the thermoacoustic coupling system are first studied. A numerical solver is used to solve the eigenvalue problem.

Considering the following physical parameters: duct length L=0.75m, height h=0.045m, reflection coefficients R_0=1 (rigid), R_L=−1 (soft boundary), flame interaction coefficient n=1, delay time τ=2ms, sound speed in the air c=345m/s, constant temperature 297K, and air density ρ_0=1.2kg/m^3. The complex eigenfrequencies (thermoacoustic modes, marked by green blocks) are plotted in Fig. 2, which show the variation of the growth rate (GR) with respect to the modal frequency of the first few low-order modes. A positive GR signifies an instable state of the system under corresponding modal frequency. These modes are, in principle, all coupled modes. However, they are tidily related to and most of time dominated by either acoustic modes or the flame intrinsic modes. Theoretically, when n reduces and tends to zero, the GR of the intrinsic dominated mode tends to negative infinity, which evolves a stable mode. Meanwhile, the GR of acoustic dominated modes will tend to zero, and finally retreat to pure acoustic modes. To figure out the nature of the mode types, the flame interaction coefficient n is gradually reduced from 1 to 0.1, and the corresponding root variation trajectories are marked by arrows in Fig.2. The GRs of the 2nd and 5th thermoacoustic modes decrease significantly, and that of modes 1, 3, 4 and 6 tend to zero. This suggests that the 2nd and 5th modes are flame controlled intrinsic modes (called I-C modes), for which a reduced n allows stabilizing the modes, whilst the rest are duct controlled acoustic modes (called A-C modes).

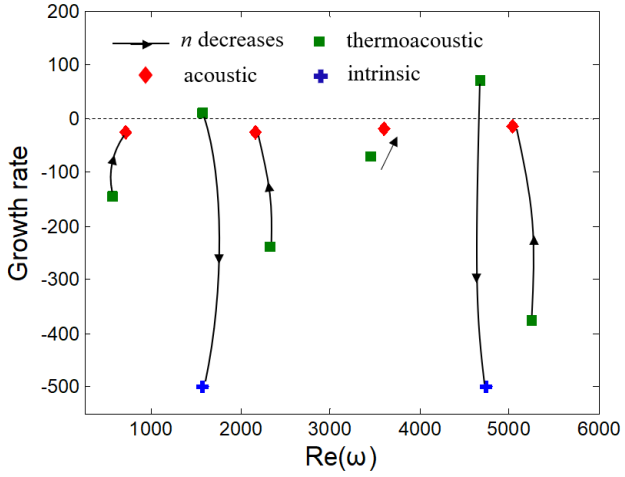

Fig. 2. Eigenfrequency trajectory distributions with varying flame interaction index n from 1 to 0.1, τ=2ms.

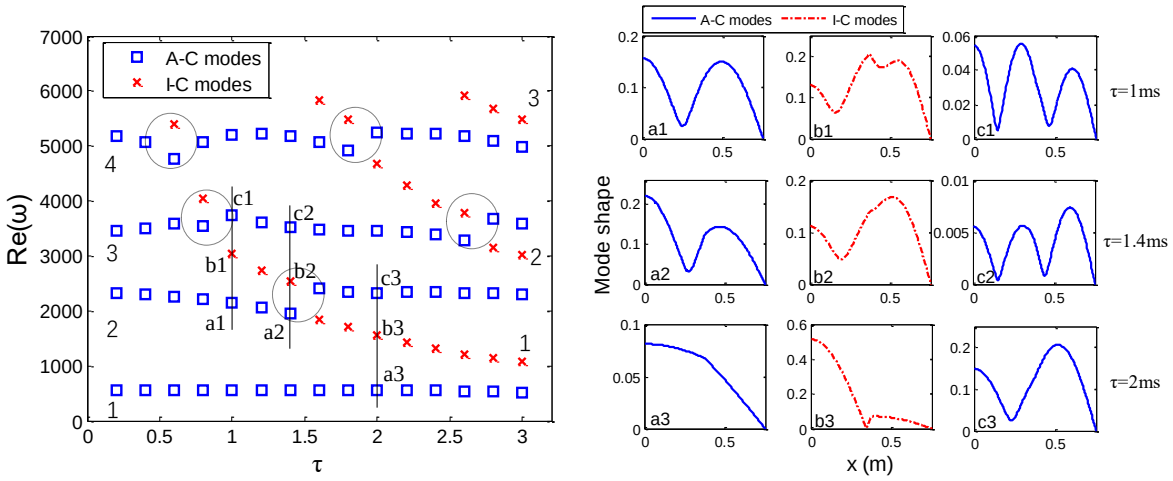

(a) (b)

Fig.3. Modal characteristic analysis. (a) Real part of eigenfrequencies for different time-lag τ, with n=1. (b) Sound pressure distribution of the A-C and I-C modes with τ =1, 1.4 and 2ms.

Fig.2 also shows that the interaction index has little effect on the vibration frequency of the I-C modes, while for an uncoupled intrinsic mode, its growth rate mainly depends on the flame interaction index. For the n-τ flame model, the time-lag τ directly affects the intrinsic modal frequencies, and further modifies the coupling behavior between the A-C and I-C modes. This is shown in Fig.3(a) by varying τ and keeping n=1 for the frequency range below 6000 rad/s. The symbols "×" in red denotes the I-C modes and the "□" in blue means the A-C modes. It can be seen that the first four coupling modes are all A-C modes for a small τ (τ<0.5). When increasing τ, more I-C modes appear in the low frequency range. Whenever a I-C mode encounters an A-C mode as marked in circles in Fig.3(a), significant coupling occurs, leading an obvious change in the modal frequencies.

Three groups of eigenfrequencies are selected from Fig. 3(a), i.e., τ = 1, 1.4 and 2ms. The corresponding mode shapes are plotted in Fig. 3(b). Among them, b1, b2 and b3 denote the I-C modes, and the other are A-C modes. Due to the coupling with the heat source, the A-C mode shapes, in terms of sound pressure distribution, show obvious asymmetry along the duct length direction. The corresponding pressure distribution of each I-C mode is related to and resembles the mode shape of its adjacent acoustic mode. For example, the mode shape b1 is due to the mutual effect of a1 and c1, while b2 behaves like the second A-C mode shape, namely a2. This is understandable since the I-C mode is caused by the local feedback loop in the vicinity of the

flame area, acting as an equivalent excitation source, thus exciting the sound field of the nearby A-C mode. The analyses confirm that the mode shape and the natural frequency of an I-C mode are significantly influenced by the A-C modes through the formation of standing-waves inside the duct. This makes it is possible to control I-C mode instabilities via properly altering the A-C modes.

3.2. Thermoacoustic instability control

Locally resonant flexible membranes are induced on the duct wall as a possible means to control the thermoacoustic instability of the system. In addition to the aforementioned I-C modes and A-C modes, the addition of the control device, i.e. the membranes in the present case, introduces the so-called membrane-controlled modes, abbreviated as M-C modes in short, whose modal frequencies and the corresponding system response are mainly dominated to the membrane vibration.

3.2.1. Characteristics of vibro-acoustic system

Properties of the vibro-acoustic system, in the absence of the flame, is first analyzed, which paves the way forward for subsequent analyses when the full thermo-vibro-acoustic coupling is considered.

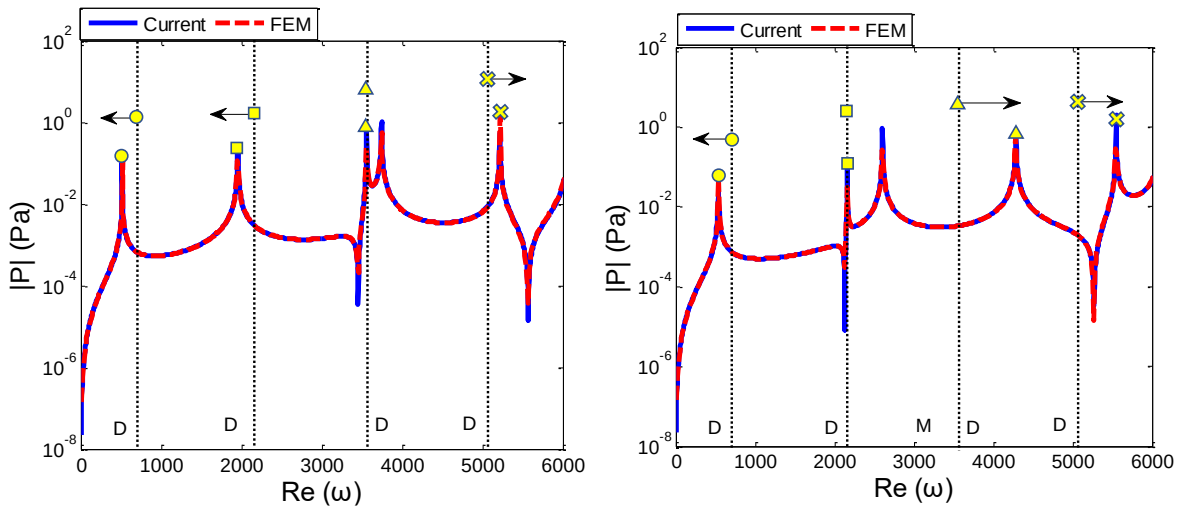

(a) (b)

Fig. 4. Sound pressure response for the duct-membrane coupling system: (a) membrane position (0.1m, 0.2m); (b) membrane position (0.2m, 0.3m)

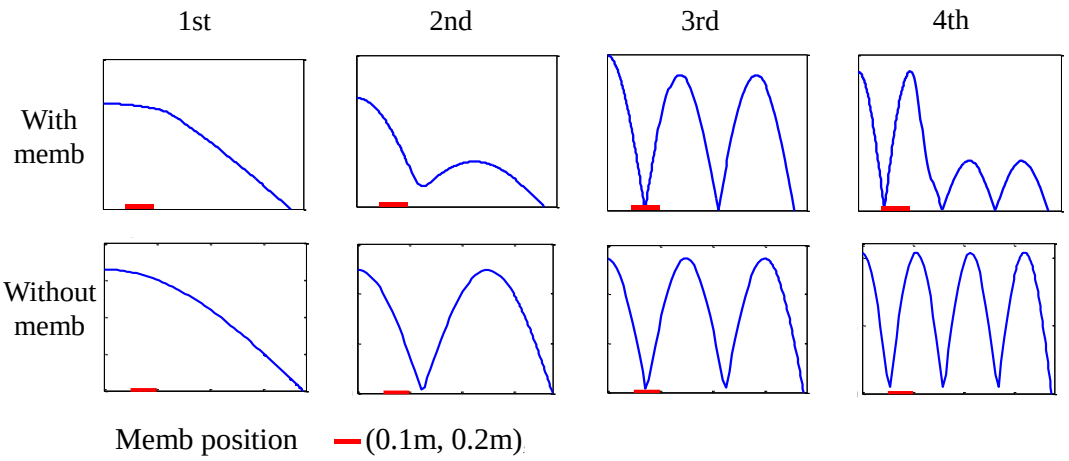

Fig. 5. The first four A-C mode shapes of the duct, with (upper row) and without (bottom row) membrane.

Using the same duct parameters as above, two flexible membranes are flush-mounted over the duct sidewall as depicted in Fig.1. Properties related to the stretched membranes are: dimensionless tension $T^*=T/\rho_0c^2h=0.1$, dimensionless mass density $m^*=\rho_m/\rho_0h$ =1, and membrane length L_m=0.1m. A unit point force is applied on the membrane at $3/5L_m$. Sound pressure response in the duct at (0.71m, 0.0223m) is presented in Fig. 4, with the blue solid line from the current model and the red dotted line from the FEA simulation. COMSOL Multiphysics® is used for FEA simulations. In the modeling, Pressure Acoustics and Truss modular are used to simulate the sound field and the 1-D membrane structure, respectively. Normal Acceleration and Edge Load are applied to describe the coupling between the membrane and the acoustic field in the duct. Subgraphs (a) and (b) show the sound pressure responses under two different membrane positions (0.1m, 0.2m) and (0.2m, 0.3m), respectively.

In the figures, vertical dashed lines represent natural frequencies of the duct (D) without membrane. Resonant frequencies before and after the deployment of the membrane are marked by symbols. The peaks without symbol correspond to the resonant frequencies dominated by the membrane. Figure 5 shows the first four acoustic mode shapes of the duct (before and after coupling with the membrane). Examining Figs.4 and 5 shows that when the membrane is located near the node of a mode, corresponding mode frequency is barely affected, such as the

third peak in Fig.4(a).

Compared with the duct natural frequencies (before coupling), the addition of the membrane seems to separate the resonance frequencies further apart, namely reducing the low-order resonant frequencies (such as the 1st and 2nd ones) and increasing the higher-order frequencies (such as 3rd and 4th ones). The introduction of a flexible structure over the rigid wall of the duct brings about two effects: stiffness effect and sound reflection. At a frequency lower than the membrane resonant frequency, the membrane offers little sound reflection but with dominant stiffness effect. In this case, the acoustic resonant frequency will be lowered after the inclusion of the membrane. When frequency approaching the sound refection band of the membrane, reflection effect is dominant, then the acoustic resonance will be shifted to higher frequency.

3.2.2. Control mechanism of the A-C mode instability

Introducing the linear n-τ model with unsteady heat release, the thermoacoustic system contains both A-C and I-C modes, which can be theoretically instable. In order to explore the controllability and the underlying mechanism, the instability of A-C modes is first studied in this section. By considering a small time-lag τ=0.5ms, only A-C modes exist below 6000rad/s as shown in Fig. 3(a). The distribution of the system eigenfrequencies is shown in Fig.6(a). The z-value marked in this figure is the determinant value of the coefficient matrix in Eq. 28. Rendering it to zero yields the eigenfrequencies of the first four A-C modes. The x-coordinate denotes the real part of ω, *i.e.*, the modal frequency, and the imaginary part is the modal stability GR. Fig.6(b) shows the sound pressure distribution. Comparing the modal stability and sound pressure distribution, it can be seen that the system is stable when the flame is located at the pressure drop (PD) region, but instable at the pressure rise (PR) part.

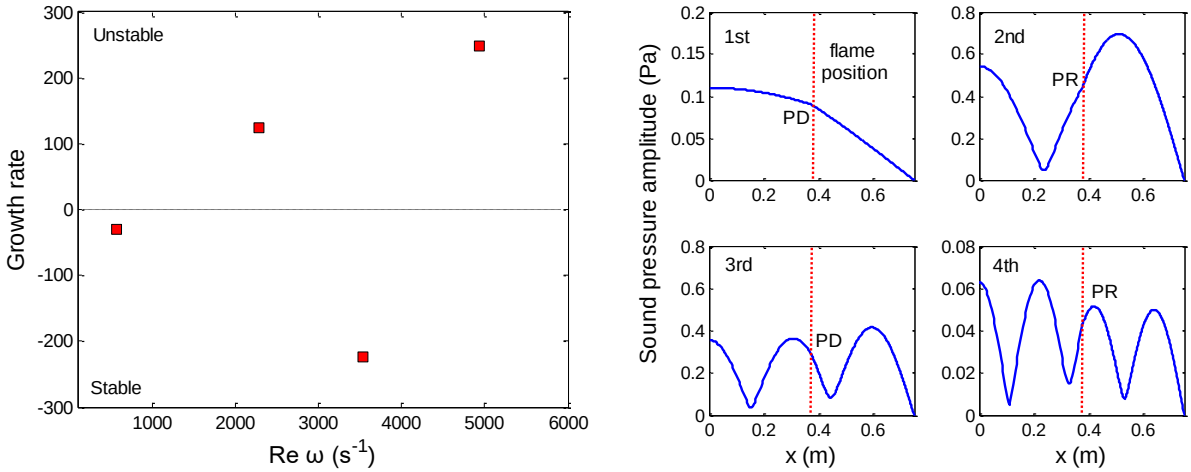

(a) (b)

Fig. 6. Modal characteristics of the thermoacoustic system (a) Eigenfrequency distribution, (b) Mode shapes of the first four A-C modes

Correlations between the observed phenomenon and Rayleigh criterion is discussed as follows. According to the Rayleigh criterion, the system is unstable when the thermoacoustic power generation ΔE is positive [37]. Related formulation is presented in Appendix A. For the present system, the values of ΔE are calculated for different flame positions, by defining $\Delta E'=\text{sign}(\Delta E) \times \log(10/|\Delta E|)$, where $\Delta E'$ has the same sign with ΔE, thus indicating the stability property with the value indicating the level. The growth rates, $\Delta E'$ and the acoustic mode shapes (before the coupling with the heat source) are shown in Fig.7 below for the first four acoustic modes. Shadow areas denote the instable regions predicted using the proposed stability criteria in terms of PD and PR. It can be seen that the results are in agreement with the Rayleigh criterion. More details about the link of current PD-PR criterion and Rayleigh criterion are depicted in Appendix A. The proposed stability criterion (PD-PR) can be regarded as an alternative interpretation of the Rayleigh Criterion. One of the advantages is that the instability can be determined in a more intuitive manner based on variations of basic acoustic quantities, which is also conducive to conceiving and understanding different control strategies, such as demonstrated in the paper using flexible membranes.

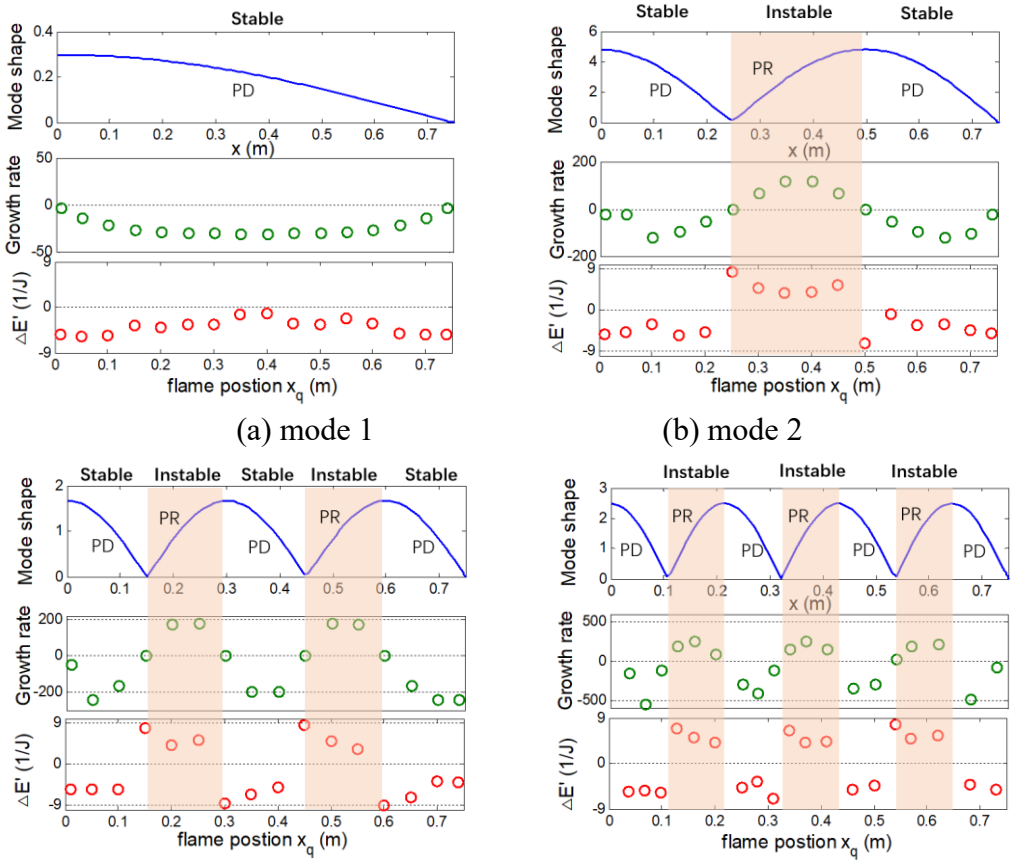

Fig.7. Modal characteristics and instability analysis for different flame positions.

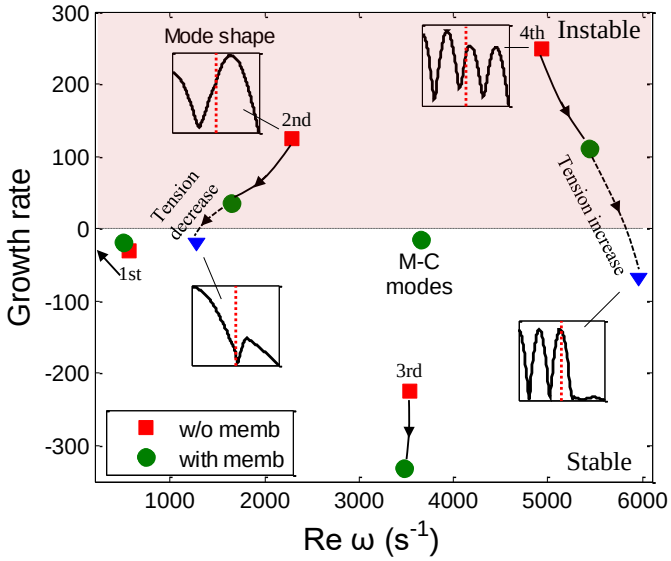

Fig. 8. Modal instabilities control using a membrane with position (0.4m, 0.5m)

The above analyses suggest that the modal instability control can be achieved by altering the

process of the pressure drop (PD) or pressure rise (PR) near the flame position, which is equivalent to stretch or compress the mode shape distribution within the flame area. In light of this, a flexible membrane is introduced into the thermoacoustic system at (0.4m, 0.5m), the effect of which on the different modes is shown in Fig. 8. In the figure, the red squares and green circles denote the eigenfrequencies before and after the membrane is deployed. A membrane-controlled mode (M-C mode) is also marked in the figure, whose stability is affected by its nearby A-C modes. Since the 3rd A-C mode is highly stable, then the newly introduced M-C mode is also stable as shown in this figure.

The frequency shift phenomenon of A-C modes when coupled with a membrane has been discussed in Fig.5. On the top of that, the GRs of the 2nd and 4th modes are significantly reduced by the membrane, demonstrating its control potential. Observing the trend of the frequency variation, it can be found that the 2nd A-C mode wavelength increase which is equivalent to a stretching of its mode shape. While for the 4th A-C mode, the mode shape is compressed.

Based on the above observation, we can further vary the tension applied to the membrane to further alter the mode shapes, which would allow adjusting its pressure state (PD or PR) near the flame position. As shown in Fig.8, reducing the membrane tension to 0.05, the 2nd A-C mode finally reaches a stable state as marked by a triangular. Similar phenomenon takes place for the 4th mode (increasing membrane tension to 0.15). Therefore, a proper choice of the membrane parameters allows tactically targeting different modes in views of instability suppression. Simultaneous control of multiple modes requires the use of a set of suitably designed membrane parameters.

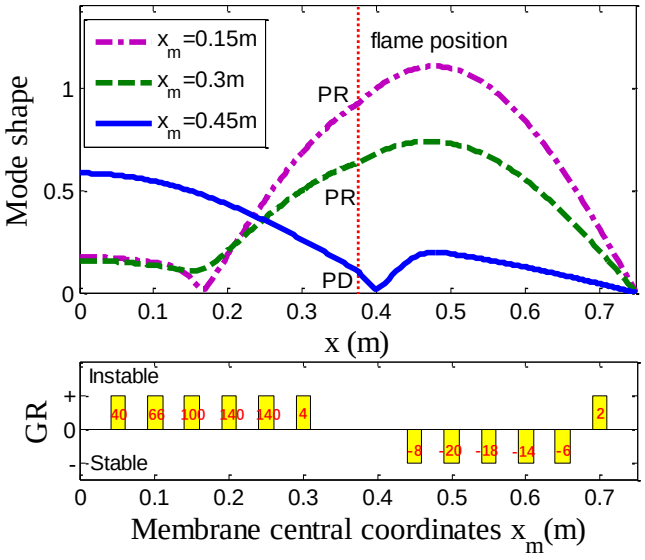

(a)

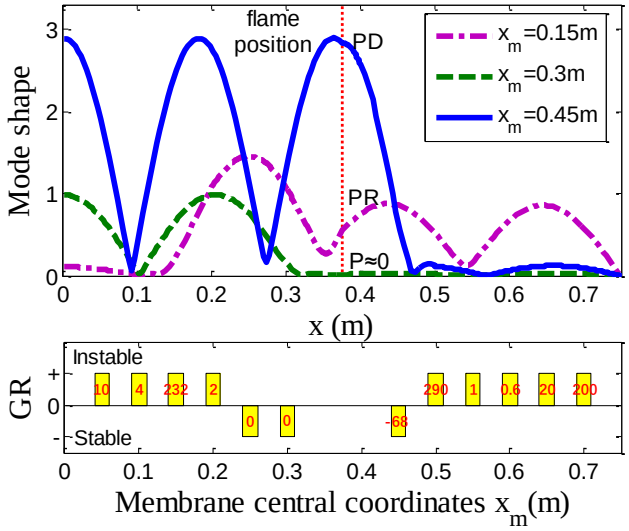

(b)

Fig. 9. Thermoacoustic instability control for the A-C modes with various membrane positions (a) 2nd, T^*=0.05, (b) 4th, T^*=0.15;

The influence of the membrane position on modal instability control is studied in Fig.9. Subgraphs (a) and (b) apply to the second and the fourth A-C modes, respectively, with a respective dimensionless membrane tension of 0.05 and 0.15. The bar-plot at the bottom denotes the modal stability GR with varying membrane position, in which the x-axis corresponds to center coordinate of the membrane x_m. Note the case of heat source right above the membrane is not considered, so GR in x_m=0.325m-0.425m are not given in this figure. The

curves in the upper figure correspond to mode shapes with different membrane positions, namely x_m=0.15m, 0.3m and 0.45m, respectively. The vertical red dashed line indicates the flame position.

For the second A-C mode, the optimal placement position is about 0.4m-0.65m after the heat source, close to the maximum pressure amplitude region. This can be understandable from that the coupling strength between the membrane and the acoustic field determines the control effect of modal instability, which is directly reflected in the pressure wave work term W_p as shown in Eq.12. The pressure amplitude determines the level of W_p as shown in Eq.14, suggesting that an effective control can be achieved when the membrane is near the maximum pressure region. When the membrane is placed before the heat source, especially around the mode shape node, the vibro-acoustic coupling between the membrane and the acoustic field inside the duct is not strong enough to alter the pressure distribution of the mode so that the flame is still in the PR area. Similar analysis and observation also apply to the fourth A-C mode, shown in Fig.9(b), giving a different optimal placement position around the flame, i.e., 0.25m-0.45m. Again, the proper location of the membrane effectively adjusts the pressure state from PR to PD so that the mode is tuned to be stable.

As a short summary, the essence of the A-C mode stability control is through the direct alteration of the acoustic modal pressure distribution inside the system. An effective control of the A-C modes relies on two-fold factors: an effective coupling between the membrane vibration and the acoustic field inside the duct, and a proper deployment of the membrane so that the acoustic pressure distribution of the A-C modes can be positively altered in the vicinity of the heat source to generate the favorable PD scenario. The above can be readily achieved through a proper design of the membrane parameters as well as its deployment location.

3.2.3. Control mechanism of the I-C modal instability

Control effect on the I-C modal instability using membranes is studied hereafter. Increasing the flame time-lag τ to 2ms, I-C modes appear below 6000rad/s as shown in Fig.3(a). All other parameters in the system still remain the same as used before. The eigenfrequencies of the

thermoacoustic system are given in Fig. 10(a), in which the 2nd and 5th modes are identified as I-C modes. Corresponding mode shapes are plotted in Fig.10(b), with the flame position marked by a vertical line. Obviously, the presence of the I-C modes makes the analysis more complex,

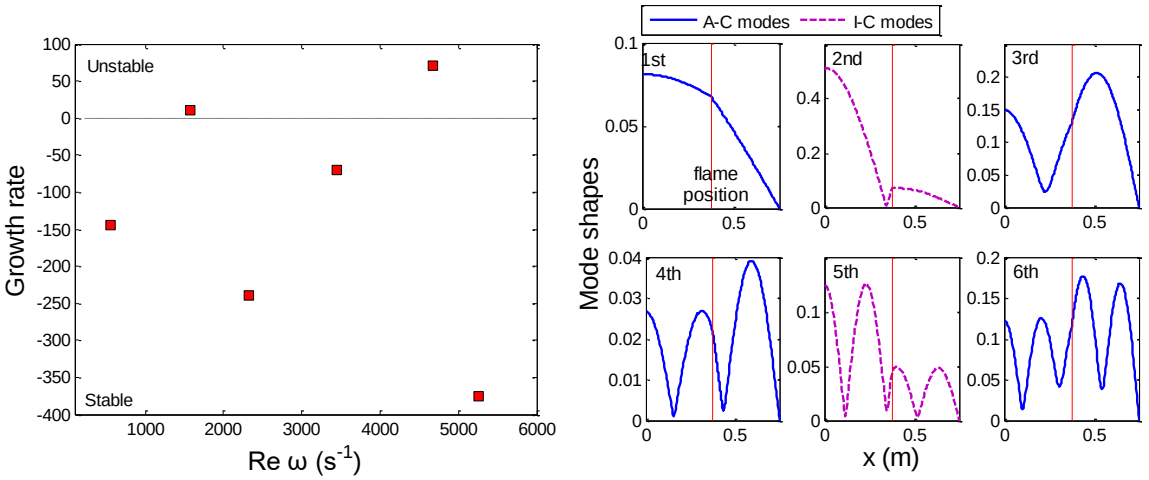

(a) (b)

Fig. 10. Study on system characteristics under the case of flame delay time τ=2ms (a) eigenfrequencies distribution; (b) mode shape.

To explore the underlying relationship between the I-C modal instability and the corresponding mode shape, the phase change in the flame transfer function (FTF), F(ω), is plotted in Fig.11 for two cases with τ=0.5ms and 2ms, respectively. F(ω) is defined as a ratio of the heat release rate fluctuation over acoustic velocity of the heat excitation, expressed as $ne^{i\omega\tau}$. For τ=2ms, the phase of the F(ω) exhibits a positive and negative variation with respect to frequency, as shown in Fig. 11. When the F(ω) phase is positive, the mode is stable and the flame is located at the PD area. Moreover, a negative F(ω) phase drives the mode into stability in the PR region as marked in the figure. This supplements the conclusions performed based on PD and PR before, and more details is presented in Appendix A. Taking the 3rd A-C mode as an example (τ=2ms), F(ω) phase is negative at its modal frequency, and the flame is located in the PR process, then the mode is stable as shown in Fig.10(a).

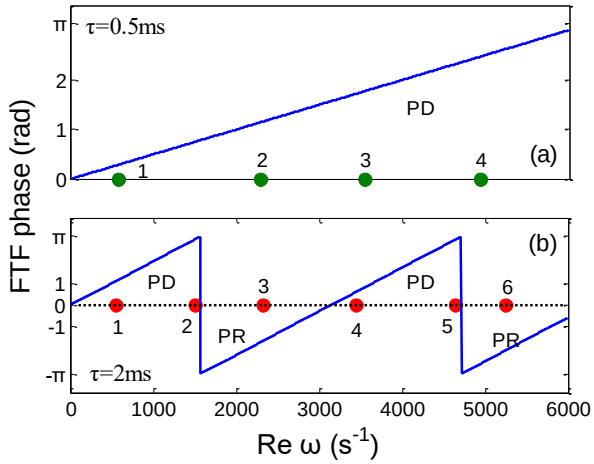

Fig.11. Phase variation of flame transfer function (FTF). The blue and red circles correspond to the natural frequencies.

Using the same flexible membrane with a dimensionless tension set to 0.1, while all other parameters remaining unchanged. Two membrane positions, one before and one after the heat source, namely (0.2m, 0.3m) and (0.4m, 0.5m), are examined. Fig. 12 compares the eigenfrequencies before and after the deployment of the membrane, for the two membrane positions in Figs. 12 (a) and (b), respectively. All three types of modes, *i.e.* M-C modes, I-C modes and A-C modes, and the corresponding distribution after control with the use of membrane are also shown in the figurers. Two instable I-C modes are marked and of particular interest for analyses. The second I-C mode seems to be easier to control in this particular case than the first I-C mode. For τ=2ms, the 2nd I-C mode is close to the 4th A-C modes, which creates strong coupling with the A-C mode as shown in Fig.3(a). The membrane can significantly change the A-C mode characteristic, then indirectly influence the coupling of A-C and I-C modes. While for the 1st I-C mode, it has weak coupling with the A-C modes, then its instability is more difficult to be altered. To understand the control mechanism behind, the influence of membrane position on the GR of the second I-C mode is shown in Fig.13 (the lower picture), and the 6th acoustic mode shape without coupling with the membrane is also given in this figure. The I-C mode remains instable at three particular positions, x_m=0.15m, 0.3m and 0.5m. It can be observed that these positions are close to the nodes of the A-C mode, evidencing a weak coupling of the membrane with the acoustic field dominated by the mode. Thus, this indirectly

confirms the acoustic field should act as a communicating agent between the membrane and the heat source which apparently determines the ultimate control effects of the I-C modes.

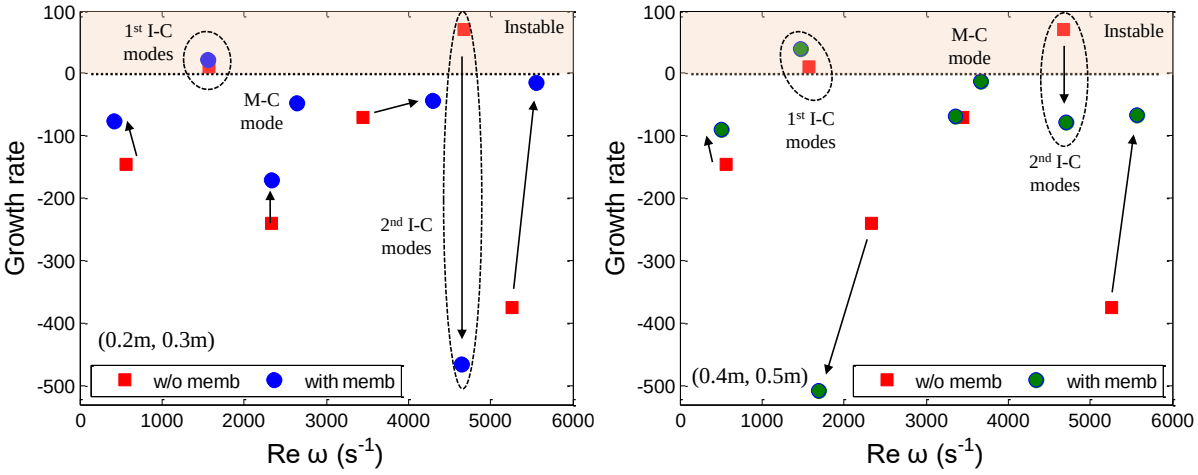

Fig.12. Instability control through the using of flexible membrane with different position. (a) (0.2m, 0.3m) (b) (0.4m, 0.5m). Keeping membrane tension as T^*=0.1.

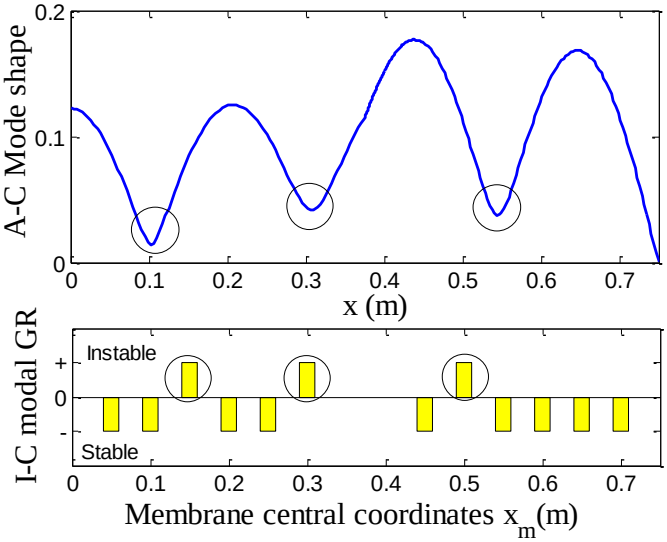

Fig. 13. Instability control mechanism of the second I-C mode with varied membrane position.

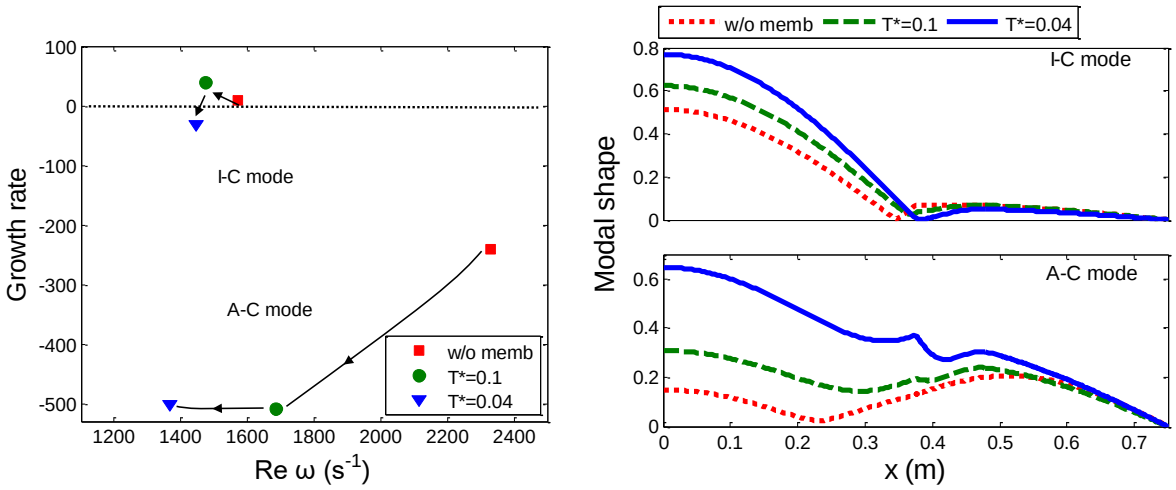

(a) (b)

Fig. 14. Influence of the membrane tension on the first I-C mode and the second A-C mode (a) eigenfrequencies distribution, (b) mode shapes

To further demonstrate this, the membrane tension is tactically adjusted in such a way that one of the duct-membrane modes approaches the first I-C mode. The analyses on Fig.4 suggests that this can definitely be achieved through effectively coupling a A-C mode with the membrane, thus also creating a strong coupling with the targeted I-C mode simultaneously. As shown in Fig. 14 (a), decreasing the membrane stiffness, the A-C mode can be shifted to lower frequency, thus stabilizing the I-C mode by the same token. Corresponding changes in the mode shape are given in Fig. 14 (b). It follows that the introduced membrane with varying tension affects more the A-C mode than I-C mode.

For the current configuration, all other modes remain stable in the frequency range of 0-6000Hz when a low tension is applied to the membrane, as presented in Fig. 15. Actually, this paper aims at revealing the control mechanism of acoustic and intrinsic modes, by focusing on some typical modes within a given low frequency band. If one wishes to achieve the best overall control effects, parametric optimizations using multiple membranes would be necessary.

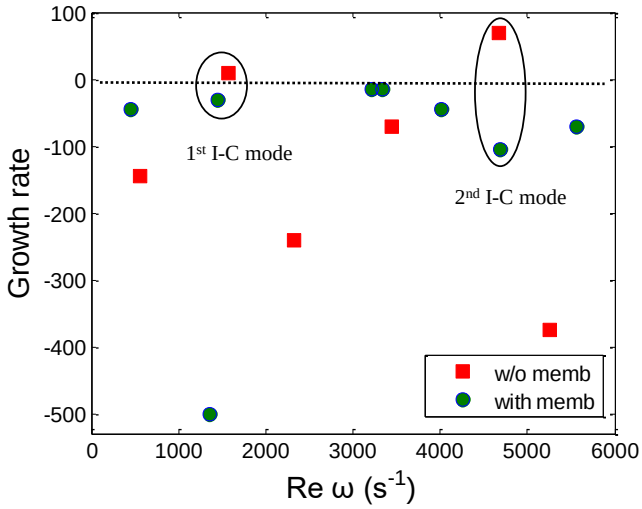

Fig.15. Instability control using a flexible membrane with a tension T^*=0.04

Successful instability control of I-C modes using membranes is achieved through a proper alteration of the acoustic field inside the duct. In this sense, the direct effects of the membrane vibration on I-C modes are rather weak. Instead, different from the control of the A-C modes, the control path is indirect and via the acoustic path through the creation of effective coupling between the acoustic field with the I-C modes. An effective coupling can be obtained through either changing the membrane tension or the applied position. This way effective temporal (frequency) and spatial (location) coupling between the acoustic field and membrane vibration can be created. The introduced membrane can change the acoustic mode shapes and the resonant frequencies, which offer a rather easy way to control thermoacoustic instability. As to the intrinsic modes, the membrane will influence the A-C modes and indirectly affect the I-C modes. Based on this concept, one can use the control device to manipulate A-C modes and further alter the targeted I-C modes.

To verify the control effect of the proposed strategy, a strongly coupled mode is considered, for which the intrinsic modes and acoustic modes might have close frequencies and thus, might strongly interact with each other. Taking the same parameters as shown in Fig. 6 in Ref. [29], τ=4.85ms, n=0.9, x_q=0.3m, contour plot $|\Lambda(\omega)|$ is presented in the Fig. 16(a). Using the membrane, the contour plot $|\Lambda(\omega)|$ is plotted in Fig. 16(b). The I-C mode stability shows obvious improvement due to the inclusion of the membrane.

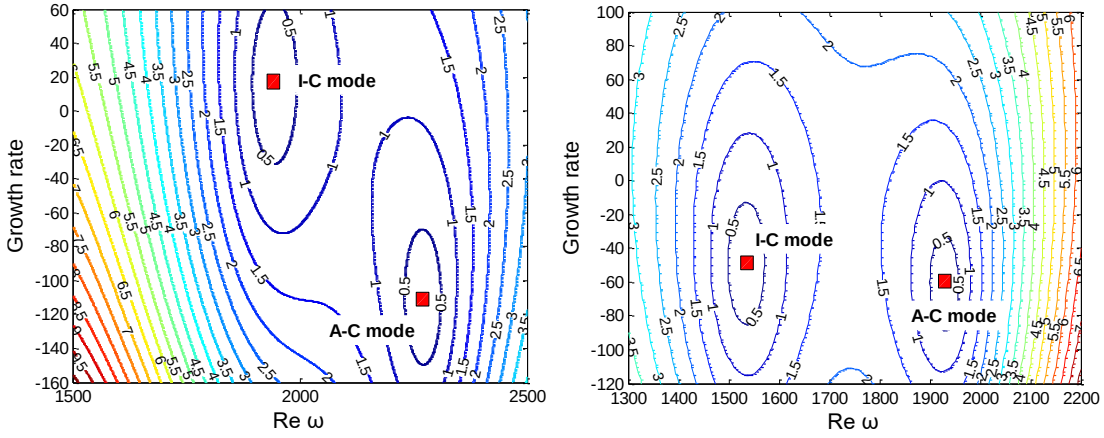

(a) (b)

Fig.16. Contour plot |Λ(ω)| without (a) and with (b) the membrane.

A few remarks need to be made before concluding. For a practical combustion system involving more complex shaped combustion chambers and flame type, the intrinsic and acoustic modes may strongly interact with each other so that they may become hardly distinguishable. Meanwhile, intrinsic modes may be affected as the flame burning state changes, or even a volume region should be considered for the flame rather than a slice. Then more adaptable control strategies or multiple control devices are needed instead of a membrane as presented in this paper. Besides, a proper choice of suitable membrane material is also an unavoidable challenge when considering possible high temperature. For aluminum which is commonly used in indoor ambient temperature environment, its dynamic properties might deteriorate in a high temperature environment such as a combustor. Alternative high temperature resistant materials, probably with high-temperature resistant coating should be considered. As to the flame description, this paper uses a traditional linear n-τ flame model, under which the effectiveness of the proposed control strategy is demonstrated. Further studies will be needed to examine the efficacy of the proposed approach under different operating environments and different flame models.

4. Conclusions

In this paper, thermoacoustic oscillation in a duct with a linear heat release n-τ model is studied. A fully coupled model, comprising the coupling among the heat source, acoustic filed

and flexible membranes on the duct wall, is established based on an energy-based formulation. This allows the computation of the system eigen-frequencies and stability metrics. Different types of eigen-modes are classified and analyzed. Intrinsic modes and acoustic modes can be distinguished through adjusting the flame interaction coefficient in the n-τ model. Modal characteristic of both A-C modes and I-C modes, their relationship with system instabilities and membrane-based controllability are thoroughly investigated.

Results show that the features of the I-C modes are directly related to n-τ flame parameters. The time-lag τ affects the intrinsic modal frequency and further governs the coupling with the acoustic modes inside the duct. An intrinsic mode shape is always tied to its adjacent A-C modes, in terms of acoustic pressure distribution. The instabilities of both the I-C and A-C modes are determined by the relationship between the flame and the acoustic mode shape. Considering different delay times, the proposed instability criterion in terms of PR and PD is shown to be in agreement with Rayleigh criterion.

The thermoacoustic instability of the system can be controlled using locally resonant membranes, flush-mounted on the duct wall with proper tension at proper locations. The underlying control mechanisms, however, are different for A-C and I-C modes. A-C mode stability control relies on the direct alteration of the acoustic modal pressure distribution inside the system. This involves a twofold process: an effective coupling between the membrane vibration and the acoustic field inside the duct, and a proper deployment of the membrane so that the acoustic pressure distribution of the A-C modes can be positively altered in the vicinity of the heat source to generate the favorable pressure state scenario (PD for a small τ). As to the control of I-C modes, since the direct effects of the membrane vibration on I-C modes are rather weak, a successful control is indirectly materialized via the acoustic path through the creation of effective coupling between the I-C modes with the nearby A-C modes. For both type of modes, the expected effects can be achieved through properly adjusting the physical parameters of the membranes and their installation locations.

Acknowledgements

This work is supported by the Research Grant Council of the Hong Kong SAR (PolyU 152036/18E), National Natural Science Foundation of China (Grant no. 11972125).

Appendix A. Rayleigh criterion and phase analyses

A.1. Rayleigh criterion

The energy power generated by the heat source can be obtained by integrating the time average of the acoustic intensity over the surface surrounding a control volume, as follows [37]:

$$\Delta E = \frac{\gamma - 1}{2 p_0 \gamma} \mathrm{Re}\left(\int_s p q' \cdot \mathbf{n} dS \right) \tag{A.1}$$

in which **n** is a unit vector pointing radially away from the heater surface *S*; *p* is the fluctuating pressure, q' is the heat release rate. According to Rayleigh criterion, the system is unstable when ΔE is positive. Therefore, instability is determined by the product of *p* and q'.

Knowing the system is very complex with the addition of membrane, it is impossible to derive a full set of analytical solutions. Nevertheless, we also tried to qualitatively address the link of PD-PR criterion and Rayleigh criterion through analytical derivations as much as possible. The acoustic pressure and the particle velocity upstream of the flame can be expressed, respectively as

$$p = A' \mathrm{e}^{-\mathrm{i}kx} + B' \mathrm{e}^{\mathrm{i}kx}, \qquad v = \frac{A'}{\rho c} \mathrm{e}^{-\mathrm{i}kx} - \frac{B'}{\rho c} \mathrm{e}^{\mathrm{i}kx} \tag{A.2a, 2b}$$

in which, the acoustic wave number $k=k_r+k_i\mathrm{i}=\omega_r/c+\mathrm{i}\omega_i/c$. Using acoustically hard-wall boundary conditions (adopted in our case), one has $A'=B'$. The above equations become

$$p = A' \left[\left(\mathrm{e}^{k_i x} + \mathrm{e}^{-k_i x} \right) \cos(k_r x) + \mathrm{i} \left(-\mathrm{e}^{k_i x} + \mathrm{e}^{-k_i x} \right) \sin(k_r x) \right] = A' \left[S_1 + S_2 \right] \tag{A.3}$$

$$v = A' / \rho c \left[\left(\mathrm{e}^{k_i x} - \mathrm{e}^{-k_i x} \right) \cos(k_r x) + \mathrm{i} \left(\mathrm{e}^{k_i x} + \mathrm{e}^{-k_i x} \right) \cos(k_r x + \frac{\pi}{2}) \right] = A' / \rho c \left[Q_1 + Q_2 \right] \tag{A.4}$$

The heat release rate is expressed as

$$q' = \frac{\bar{\rho} \bar{c}}{\gamma - 1} n \mathrm{e}^{\mathrm{i}\omega\tau} v \delta(x - x_q) \tag{A.5}$$

In the current model, some simplifications on the pressure and velocity are adopted to estimate the power ΔE by ignoring the small terms, such as S_2 and Q_1. Indeed, the values of S_1, S_2, and Q_1, Q_2 are plotted in Fig. A.1 for the second and third acoustic modes, chosen as illustrative examples. It can be seen that Q_1 and S_2 are indeed very small terms. Verifications on other modes discussed in this paper also show the same conclusion, the results of which are

not presented here.

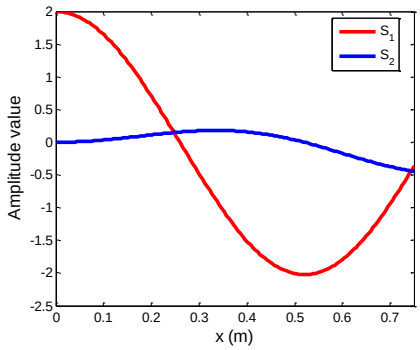

(a) S_1 and S_2 distribution for mode 2

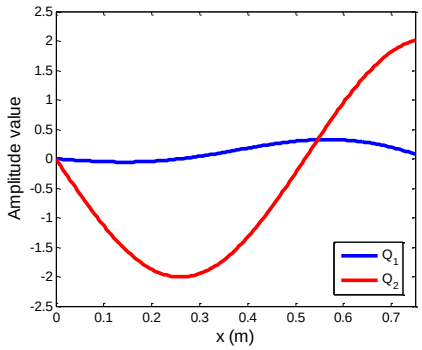

(b) Q_1 and Q_2 distribution for mode 2

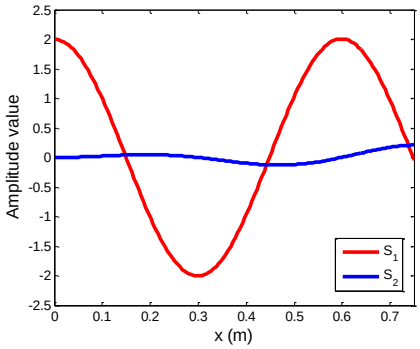

(c) S_1 and S_2 distribution for mode 3

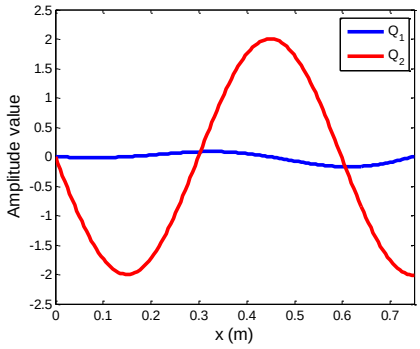

(d) Q_1 and Q_2 distribution for mode 3

Fig. A.1. The distributions of S_1, S_2, and Q_1, Q_2 in the expressions of pressure and velocity.

Combining Eqs. A.1-A.5 and ignoring S_2 and Q_1 in Eqs. A.3 and A.4, approximated ΔE, denoted as ΔEs, can be obtained as

$$\Delta Es = \frac{(A')^2}{2p_0\gamma} n \sin(\omega\tau)\left[\left(e^{k_i x} + e^{-k_i x}\right)^2 \cos(k_r x)\cos(k_r x + \frac{\pi}{2})\right] \tag{A.6}$$

To further verify the correctness of using ΔEs to predict the thermoacoustic power, ΔEs and ΔE obtained from Eqs. A.1 and A.6, respectively, are compared. Taking the second and third modes again as an example, the absolute value and the sign of ΔEs and ΔE are shown in Fig.A.2 for different flame positions. It can be seen that they carry the same signs and have close values, thus proving the above simplification is indeed acceptable.

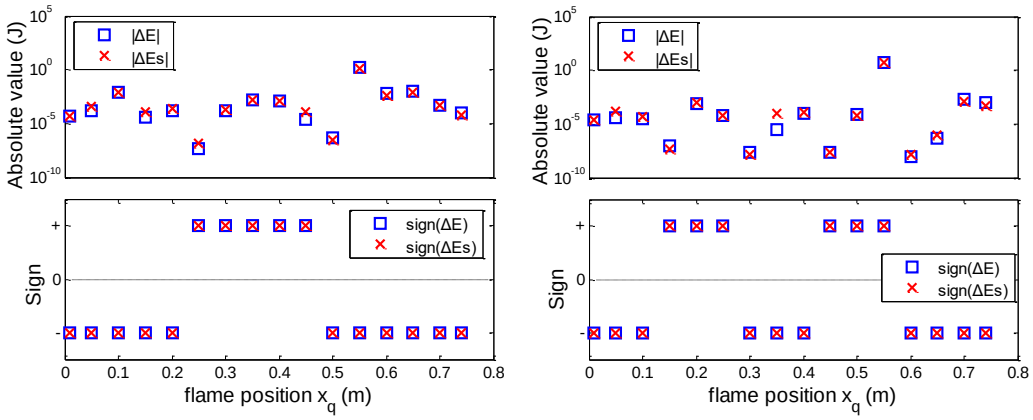

(a) mode 2 (b) mode 3

Fig. A.2. Comparisons of the absolute value and the sign of ΔEs and ΔE

In Eq.A.6, as $\omega\tau \in (0, \pi)$, $\sin(\omega\tau)>0$, for $\Delta E<0$ (stable), the last two terms $\cos(k_r x)$ and $\cos(k_r x+\pi/2)$ should carry opposite signs. The term $\cos(k_r x)$ can be regarded as the spatial distribution of pressure wave, and $\cos(k_r x+\pi/2)$ corresponds to the velocity, whose values are plotted in the Fig. A.3 for the 2nd acoustic modes as an example. When considering $|\cos(k_r x)|$, the unstable region plotted in Fig.A.3 is PR (pressure rise) region and the stable region corresponds to PD (pressure drop) region.

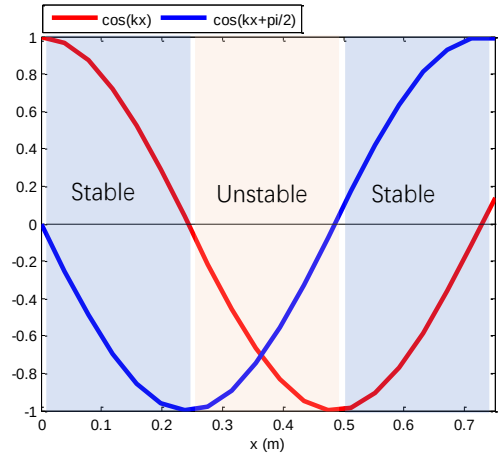

Fig. A.3. The distributions of $\cos(k_r x)$ and $\cos(k_r x+\pi/2)$

For a larger delay τ, $\sin(\omega\tau)$ in Eq. A.6 can be negative. Then the specific range of $\omega\tau$ should be studied as presented in Fig.11. For τ=0.5ms and ω varying from 0-6000 rad/s, $\omega\tau \in (0, \pi)$. In this case, when the flame placed in the PD region, the system will be sable. As τ increases to 2ms, different regions for $\omega\tau \in (0, \pi)$ or $(-\pi, 0)$ are shown in Fig.11. It indicates that when $\omega\tau \in$

(-π, 0), for ΔE<0 (stable) in Eq.A.6, the last two terms cos($k_r x$) and cos($k_r x$+π/2) should carry the same signs, then PR will be the stable region. Therefore, the proposed stability criterion (PD-PR) is again consistent with and closely related to the Rayleigh criterion.

A.2. Phase analysis

Under the plane wave assumption, the fluctuating pressure, velocity and heat release rate in a duct can be expressed:

$$p = A'\mathrm{e}^{-\mathrm{i}k^- x} + B'\mathrm{e}^{\mathrm{i}k^- x} = |p| e^{i\theta_1} \tag{A.7}$$

$$v = \frac{A'}{\rho^- c^-}\mathrm{e}^{-\mathrm{i}k^- x} - \frac{B'}{\rho^- c^-}\mathrm{e}^{\mathrm{i}k^- x} = |v|\mathrm{e}^{i\theta_2} \tag{A.8}$$

$$q' = \frac{\rho^- c^-}{\gamma - 1} n\mathrm{e}^{\mathrm{i}\omega\tau} v\delta(x - x_q) = |q'|\mathrm{e}^{\mathrm{i}\omega\tau}\mathrm{e}^{\mathrm{i}\theta_2} \tag{A.9}$$

The above expressions show the amplitude and phase of these physical quantities. Then the Rayleigh criterion can be described as

$$\Delta E = \frac{\gamma - 1}{2 p_0 \gamma}|p||q'|\mathrm{Re}\left(\mathrm{e}^{i\omega\tau}\mathrm{e}^{i\theta_1}\mathrm{e}^{i\theta_2}\right) \tag{A.10}$$

The above equation can be further simplified as

$$\Delta E = \frac{\gamma - 1}{2 p_0 \gamma}|p||q'|\mathrm{Re}\left(\mathrm{e}^{i\omega\tau}\mathrm{e}^{i\theta_1}\mathrm{e}^{i\theta_2}\right) = \frac{\gamma - 1}{2 p_0 \gamma}|p||q'|e^{-\omega_i\tau}\cos(\omega_r\tau + \theta_2 + \theta_1) \tag{A.11}$$

It can be seen that the sign of ΔE is determined by cos($\omega\tau$+θ_2+θ_1), in which the term $\omega\tau$+θ_2 belongs to the phase of the heat release rate. θ_1 represents the phase of the pressure fluctuation. Considering the flame as being equivalent to a volume velocity source and according to the mass conservation principle around the flame, one has [6]

$$\rho v\Big|_{x=x_q^+} - \rho v\Big|_{x=x_q^-} = \frac{(\gamma - 1)}{(c^-)^2} q' = Q_{down} \tag{A.12}$$

The right-hand side term can be seen as the downstream-traveling mass flow or velocity generated by the flame. Then the upstream-traveling mass flow can be described as $-Q_{down}$, with a phase $-(\omega\tau + \theta_2)$. When the pressure fluctuation has the same phase as the upstream-traveling mass flow, i.e. $-(\omega\tau + \theta_2) = \theta_1$, ΔE>0 and instability occurs.

Appendix B. Temperature jump across the heat source

When considering a temperature jump across the flame (from T_1 to T_2), its effects on air density and the sound speed should be considered in Eqs. 6 and 7. They become

$$A'\mathrm{e}^{-\mathrm{i}k^- x_\mathrm{q}} + B'\mathrm{e}^{\mathrm{i}k^- x_\mathrm{q}} = C'\mathrm{e}^{-\mathrm{i}k^+ x_\mathrm{q}} + D'\mathrm{e}^{\mathrm{i}k^+ x_\mathrm{q}} \tag{B.1}$$

$$\frac{1}{c^-}\left(A'\mathrm{e}^{-\mathrm{i}k^- x_\mathrm{q}} - B'\mathrm{e}^{\mathrm{i}k^- x_\mathrm{q}}\right) - \frac{1}{c^+}(C'\mathrm{e}^{-\mathrm{i}k^+ x_\mathrm{q}} - D'\mathrm{e}^{\mathrm{i}k^+ x_\mathrm{q}}) = \frac{1}{(c^-)}F(\omega)(A'\mathrm{e}^{-\mathrm{i}k^- x_\mathrm{q}} - B'\mathrm{e}^{\mathrm{i}k^- x_\mathrm{q}}) \tag{B.2}$$

in which, $c=(\gamma \mathrm{R_g} T)^{1/2}$, $k=\omega/c$, γ is the ratio of specific heat and $\mathrm{R_g}$ is the universal gas constant. Positive and negative sign correspond to the two temperature regions respectively. Meanwhile, if the control membrane is applied to the downstream of the flame, the air density and sound speed in Eq. 15 should be revised as

$$p_{\mathrm{rad}}(x,y) = \frac{\rho^-}{2h}\sum_{m=0}^{\infty}\frac{\omega}{k_m^-}\psi_m(y)\int_0^{L_\mathrm{m}}\psi_m(y_\mathrm{s})\Big|_{y_\mathrm{s}=0}\mathrm{i}\omega u \times G(x,x')\mathrm{d}x' \tag{B.3}$$

in which $\rho = p/\mathrm{Rg}T$, p is the static pressure.

Taking the same parameters as Fig. 8, a temperature jump (T_1 and T_2 across the heat source) is considered before and after the flame, with T_1=297K, T_2=488K and T_1=297K, T_2=788K, T*=0.05, respectively. In Fig. B.1, the red squares and green circles denote the eigenfrequencies before and after deploying the membrane, respectively. The effectiveness of the instability control can be observed. In the subsequent study, a more complex case (including the coupled intrinsic modes) is considered, using τ=3ms, x_q=0.2L, T_1=297K, T_2=488K, membrane tension T*=0.15, at position (0.05m,0.15m). Keeping other parameters unchanged, a comparison of modal instabilities with and without the membrane are presented in Fig. B.2. Obvious control effect can be seen, which proves the effectiveness of the proposed method and model even when a temperature jump exists.

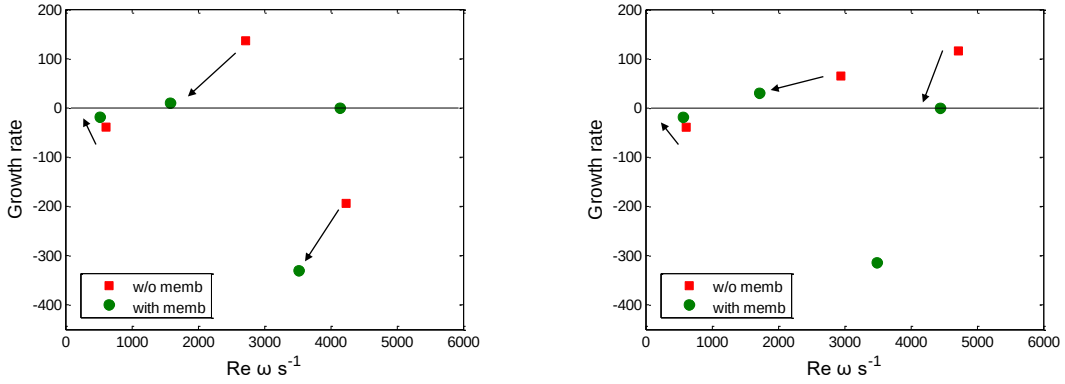

(a) T_1=297K, T_2=488K (b) T_1=297K, T_2=788K

Fig. B.1. Modal instabilities control using a membrane with the consideration of temperature jump.

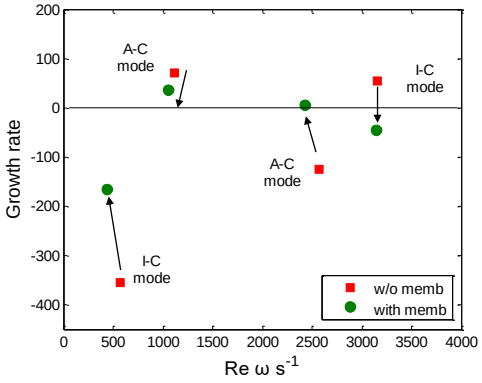

Fig. B.2. Modal instabilities control using a membrane with n=1, τ=3ms, x_q=0.2 L, T_1=297K, T_2= 488K, membrane position (0.05m, 0.15m), tension T*=0.15

References

[1] F. E. C. Culick, V. Yang, Prediction of the stability of the unsteady motions in solid propellant rocket motors, AIAA J. 143 (1992) 719-779.

[2] T. Lieuwen, H. Torres, C. Johnson, B.T. Zinn, A mechanism of combustion instability in lean premixed gas turbine combustors, J. Eng. Gas. Turb. Power 123 (2000) 1182-1189.

[3] S. Hubbard, A. P. Dowling, Acoustic resonances of an industrial gas turbine combustion system, J. Eng. Gas. Turb. Power 123 (2001) 766-773.

[4] P. L. Rijke, LXXI. Notice of a new method of causing a vibration of the air contained in a tube open at both ends, Lond. Edinb. Dubl. Phil. Mag. 17 (1859) 419-422.

[5] L. Rayleigh, Theory of Sound (two volumes), Dover Publications, New York, 1945.

[6] A. P. Dowling, The calculation of thermo-acoustic oscillations, J. Sound. Vib.180 (1995) 557-581.

[7] A. P. Dowling, S. R. Stow, Acoustic analysis of gas turbine combustors, J. Propul. Power. 19(2003) 751-764.

[8] T. Lieuwen, Modeling Premixed Combustion-Acoustic Wave Interactions: A Review, J Propul. Power 19 (5) 2012 765-781.

[9] N. Olgac, U. Zalluhoglu, A. S. Kammer, Predicting Thermoacoustic Instability: A Novel Analytical Approach and Its Experimental Validation, J Propul. Power 30(4) 2014 1005-1015.

[10] F. Nicoud, L. Benoit, C. Sensiau, T. Poinsot, Acoustic modes in combustors with complex impedances and multidimensional active flames, AIAA. J. 45 (2) (2007) 426-469.

[11] X. Xing, Q. Xu, J. T. Du, L. Cheng, Z. G. Liu, A Modified Fourier Series Solution for a Thermo-Acoustic Tube with Arbitrary Impedance Boundaries, Int. J. Appl. Mech. 12 (05) (2020) 2050047.

[12] M. A. Heckl, Active control from the noise of a Rijke tube, J. Sound Vib.124 (1988) 117-133.

[13] A. P. Dowling, A. S. Morgans, Feedback Control of Combustion Oscillations, Annu. Rev. Fluid Mech. 37(1) (2005) 151-182.

[14] U. Zalluhoglu, N. Olgac, Deployment of Time-Delayed Integral Control for Suppressing Thermoacoustic Instabilities, J. Guid. Control Dynam. 39(10) (2016) 2284-2296.

[15] V. Bellucci, P. Rohr, C. O. Paschereit, F. Magni, On the Use of Helmholtz Resonators for Damping Acoustic Pulsations in Industrial Gas Turbines, J. Eng. Gas Turb. Power 126(2) (2004) 271-275.

[16] I. Dupere, A. P. Dowling, The Use of Helmholtz Resonators in a Practical Combustor, J. Eng. Gas Turb. Power 127(2) (2005) 268-275.

[17] U. Zalluhoglu, N. Olgac, Placement of Helmholtz resonators in series for passive control of thermoacoustic instabilities from a time-delay perspective, Proceedings of the American Control Conference (2016), 1845-1850.

[18] Z. G. Zhang, D. Zhao, N. M. Han, S. H. Wang, J. W. Li, Control of combustion instability with a tunable Helmholtz resonator, Aerosp. Sci. Technol. 41 (2015) 55-62.

[19] R. Cora, C. A. Martins, P. T. Lacava, Acoustic instabilities control using Helmholtz resonators. Appl. Acoust. 77 (2014) 1-10.

[20] L. Li, Z. H. Guo, C. Y. Zhang, X. F. Sun, A Passive Method to Control Combustion Instabilities with Perforated Liner, Chinese J. Aeronaut. 23(6) (2010) 623-630.

[21] A. Surendran, M. A. Heckl, Passive instability control by a heat exchanger in a combustor with nonuniform temperature, Int. J. Spray Combust. 9 (4) (2017) 380-393.

[22] D. Zhao, E. Gutmark, A. Reinecke, Mitigating self-excited flame pulsating and thermoacoustic oscillations using perforated liners, Sci. Bull. 64(13) (2019) 941-952.

[23] G. Y. Zhang, X. Y. Wang, L. Li, X. D. Jing, X. F. Sun, Control of thermoacoustic instability with a drum-like silencer, J. Sound Vib. 406 (2017) 253-276.

[24] M. Hoeijmakers, V. Kornilov, I. L. Arteaga, P. de Goey, H. Nijmeijer, Intrinsic instability of flame-acoustic coupling, Combust. Flame 161(11) (2014) 2860-2867.

[25] T. Emmert, S. Bomberg, W. Polifke, Intrinsic thermoacoustic instability of premixed flames, Combust. Flame 162(1) (2015) 75-85.

[26] M. Hoeijmakers, V. Kornilov, I. L. Arteaga, P. de Goey, H. Nijmeijer, Flame dominated thermoacoustic instabilities in a system with high acoustic losses. Combust. Flame 169 (2016) 209-215.

[27] N. K. Mukherjee, V. Shrira, Intrinsic flame instabilities in combustors: Analytic description of a 1D resonator model, Combust. Flame 185 (2017) 188-209.

[28] N. K. Mukherjee, Analytic description of flame intrinsic instability in one-dimensional model of open-open combustors with ideal and non-ideal end boundaries, Int. J. Spray

Combust. 10 (4) (2018) 287-314.

[29] N. K. Mukherjee, V. Shrira, Coupling of Acoustic and Intrinsic Modes in 1D Combustor Models, Combust. Sci. Technol. (2019).

[30] T. Emmert, S. Bomberg, S. Jaensch, W. Polifke, Acoustic and intrinsic thermoacoustic modes of a premixed combustor, P. Combust. Inst. 36(3) (2017) 3835-3842.

[31] A. Ghani, T. Steinbacher, A. Albayrak, W. Polifke, Intrinsic thermoacoustic feedback loop in turbulent spray flames, Combust. Flame 205 (2019) 22-32.

[32] P. E. Buschmann, G. A. Mensah, J. P. Moeck, Intrinsic thermoacoustic modes in an annular combustion chamber, Combust. Flame 214 (2020) 251-262.

[33] A. Orchini, C. F. Silva, G. A. Mensah, J. P. Moeck, Thermoacoustic modes of intrinsic and acoustic origin and their interplay with exceptional points, Combust. Flame 211 (2020) 83-95.

[34] L. X. Huang, Modal analysis of a drumlike silencer, J. Acoust. Soc. Am. 112 (2002) 2014-2025.

[35] Y. Liu, J. T. Du, L. Cheng, Bandgap Formation under Temperature-induced Quasi-periodicity in an Acoustic Duct with Flexible Walls, J. Sound Vib. 486 (2020) 115615.

[36] P. E. Doak, Excitation, transmission and radiation of sound from source distributions in hard-walled ducts of finite length (I): the effects of duct cross-section geometry and source distribution space-time pattern, J. Sound Vib. 31(1) (1973) 1-72.

[37] Y. P. Kwon, B. H. Lee, Stability of the Rijke thermoacoustic oscillation, J. Acoust. Soc. Am. 78(4) (1985) 1414-1420.

[38] J. T. Du, Y. Liu, Y. F. Zhang, Influence of boundary restraint on sound attenuation performance of a duct-membrane silencer, Appl. Acoust. 105 (2016) 156-163

[39] J. T. Du, W. L. Li, H. A. Xu, Z. G. Liu. Vibro-acoustic analysis of a rectangular cavity bounded by a flexible panel with elastically restrained edges, J Acoust Soc Am. 131 (2012) 799-810.